Journal of Coastal Research	29	6	1413–1419	Coconut Creek, Florida	November 2013

Observations of High-Frequency Internal Waves in the Southern Taiwan Strait

Xiaolin Bai[†], Zhiyu Liu[†], Xiaofeng Li[‡], Zhaozhang Chen[†], Jianyu Hu[†]*, Zhenyu Sun[†], and Jia Zhu[†]

[†]State Key Laboratory of Marine Environmental Science
College of Ocean & Earth Sciences
Xiamen University
Xiamen, Fujian 361005, China

[‡]International Center for Marine Studies
Shanghai Ocean University
Shanghai 201306, China

www.cerf-jcr.org

www.JCRonline.org

ABSTRACT

Bai, X.; Liu, Z.; Li, X.; Chen, Z.; Hu, J.; Sun, Z.; and Zhu, J., 2013. Observations of high-frequency internal waves in the southern Taiwan Strait. *Journal of Coastal Research,* 29(6), 1413–1419. Coconut Creek (Florida), ISSN 0749-0208.

Based on *in situ* hydrographic measurements at a station at about 60 m depth near the local shelf break in July 2011 and a satellite image of the sea-surface roughness, we present the evidence of existence and characteristics of high-frequency internal waves (HIWs) in the southern Taiwan Strait. Variations of the thermohaline structure at the observational site were revealed by repeating conductivity-temperature-depth (CTD) profiling measurements of every 2 hours, while fluctuations of the isothermals due to the passage of HIWs were recorded by continuous CTD measurements with a probe positioned approximately in the middle of the pycnocline. A fast sampling frequency of 8 Hz allows the structure of the HIWs to be captured in great detail. The waves were depression waves, with a period of about 6.2 min and an amplitude of about 25 m. The propagation speed of the waves is estimated to be 0.56 m/s by solving the KdV equation with the observed background stratification. The frequent occurrence of HIWs in the Taiwan Strait is evidenced by the analysis of a MODIS true color image of the sea-surface roughness. The possible generation mechanism of the HIWs is discussed based on a MODIS image and the perturbed KdV equation.

ADDITIONAL INDEX WORDS: *High-frequency internal waves, internal tide, CTD data, MODIS true color image, perturbed KdV equation.*

INTRODUCTION

The Taiwan Strait (TWS) is a shallow channel connecting the South China Sea (SCS) and the East China Sea, playing a significant role in their water exchanges. The currents in the TWS include the coastal current, the SCS Warm Current extension, and the occasional Kuroshio intrusion (Hu *et al*., 2010). The changes of these currents induce significant variations of thermohaline structures and water mass distributions.

The Taiwan Bank is located in the southern TWS immediately onshore of the local shelf break. Its topographic characteristics favor generation of high-frequency internal waves (HIWs) by tidal currents flowing over shallow banks in warm seasons, as in many other seas with similar bathymetric features (Colosi *et al*., 2001; Duda *et al*., 2004; Lee and Beardsley, 1974). Meanwhile, the seasonal pycnocline supports the generation and propagation of HIWs in this area. The HIWs are high-frequency and usually large-amplitude waves existing in stratified oceans. They affect both vertical and horizontal exchanges of mass, heat, and energy, and they induce dramatic thermohaline structure changes as they propagate through the water column (Cai *et al*., 2008).

With the advance of satellite remote-sensing technology, HIWs in the coastal and shelf seas of China have been frequently observed and reported. In particular, HIWs were often identified in the northern SCS from synthetic aperture radar (SAR) images (Li, Zhao, and Pichel, 2008; Liu and Hsu, 2004; Zhao and Alford, 2006; Zheng *et al*., 2001, 2007) and ocean color images (Cai, Xie, and He, 2012; da Silva, New, and Srokosz, 2002; Ho, Su, and Zheng, 2008; Jackson, 2007). In addition, several international experiments, such as the ASIAEX (Asian Seas International Acoustics Experiment), have concentrated on the generation, propagation, and evolution of features of the HIWs in the SCS (Liu, Zhao, and Hsu, 2008). Meanwhile, modeling of HIWs in the SCS has also been conducted by several authors (for a recent review on the topic, see Simmons *et al*., 2011). However, to our knowledge, *in situ* observations of HIWs in the TWS have not been reported in the literature. To this end, in this study, by using *in situ* hydrographic measurements at a station at about 60 m depth near the local shelf break in July 2011 and a satellite image of the sea-surface roughness, we present evidence of the existence and characteristics of HIWs in the southern TWS.

This paper is structured as follows. In the "Observations" section, we describe the observational evidences for HIWs in the southern TWS, which include the *in situ* hydrographic measurements and satellite observations. The analyses of the *in situ* measurements and the properties of the waves are

DOI: 10.2112/JCOASTRES-D-12-00141.1 received 19 July 2012; accepted in revision 30 December 2012; corrected proofs received 10 March 2013.
* Corresponding author. E-mail: hujy@xmu.edu.cn
Published Pre-print online 2 April 2013.

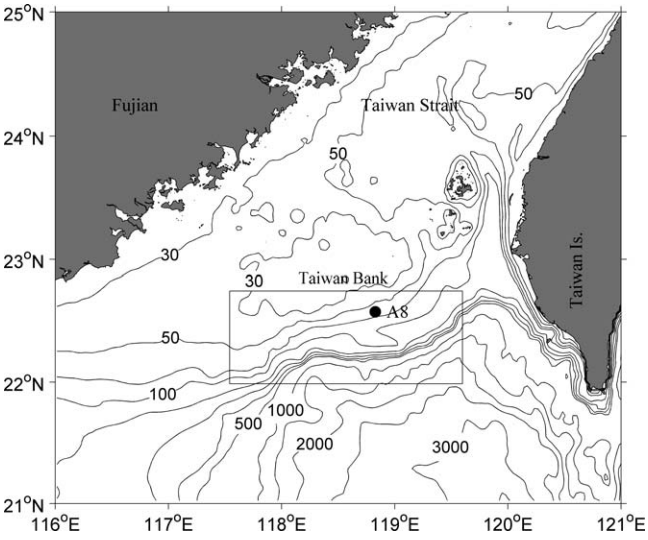

Figure 1. The location of the observational station. Sta. A8 is shown with a black dot.

Figure 2. A snapshot of the sea surface at Sta. A8. The red arrow points to the observed heap of water. (Photo taken on R/V *Yanping 2* by the second author.) (Color for this figure is available in the online version of this paper.)

presented in the "Results" section. The "Discussion" section expounds on the possible generation mechanism of the HIWs. We summarize our findings in the "Summary" section.

OBSERVATIONS

In Situ Measurements

A group of HIWs was successfully recorded during a research cruise in July 2011. As shown in Figure 1, the black dot is the position of Sta. A8, where the passage of large-amplitude HIWs was captured by *in situ* hydrographic measurements. The mean water depth is about 60 m at the station. Time-series measurements of temperature and salinity profiles were conducted using a SeaBird SBE 25 conductivity-temperature-depth (CTD) profiler for about 42 hours. As a rule, one CTD cast was taken every 2 hours, and in total 22 hydrographic profiles were obtained from 0110 UTC 11 July to 1900 UTC 12 July.

During data collections at Sta. A8, a photo of the sea surface was taken at 2121 UTC (local early morning) on 11 July 2011, when a long, well-defined heap of water apparently moving toward the research vessel was noticed (Figure 2). It was judged to be the surface signature of the propagation of HIWs, and we thus immediately started an intensive field campaign by positioning a CTD probe at a depth of about 33 m, roughly in the middle of the pycnocline. The probe was set to work in a continuous mode with a sampling frequency of 8 Hz. The measurements lasted for about 1 hour and ended when there were no noticeable vertical fluctuations of isothermals any more. In addition, temperature and salinity profiles half an hour before the arrival of the HIWs were obtained with an MSS-90L microstructure profiler. These represented the pre-HIWs background stratification at Sta. A8 and were used to estimate the propagation speed and amplitude of the HIWs.

Anticipating that HIWs may pass by Sta. A8 again after a semidiurnal tidal period, we conducted similar continuous measurements 12 hours later, but no evident HIWs were observed. Hence, the following analysis focuses on the former continuous measurements.

Satellite Observation

In addition to the *in situ* hydrographic measurements and visual observation of the sea-surface roughness, surface signatures of HIWs in the southern TWS were captured by a MODIS (Moderate Resolution Imaging Spectroradiometer) true color image taken at 0515 UTC on 8 July 2010, making the analysis of the two-dimensional structure of HIWs possible. The spatial resolution of the image is 250 m.

The principles and application of the detection of HIWs in MODIS true color images have been described by Jackson (2007). Simply speaking, although HIWs indicate the ocean's inner unrest, they modulate sea-surface current and wave fields, and thus change the sea-surface roughness, which can be detected by satellite images (Jackson, 2007; Li, Zhao, and Pichel, 2008; Liu and Hsu, 2004).

It is a pity that there are no concurrent *in situ* and satellite observations of the same high-frequency internal wave packet, but this on the other hand suggests that the occurrence of HIWs in the southern TWS is not purely episodic, but may be in a frequent, even periodic manner. Further discussions on this issue will be given in the following sections.

RESULTS

Variations of Thermohaline Structures

The temporal variations of the thermohaline structure interpolated from the 22 CTD profiles are shown in Figure 3. A typical three-layer water-column structure is evident: a thin upper mixed layer of about 8 m, a well-mixed bottom boundary layer of about 20 m, and a wide (about 30 m in thickness) pycnocline/thermocline/halocline in between. The surface-bottom temperature and salinity differences are about 9°C and 1.8, respectively. High-temperature (>28°C) and low-salinity (<32.8) water is in the upper layer, while low-temperature (<21°C) and high-salinity (>34.4) water is in the lower layers. It is evident from Figure 3a that the thermocline is between 10 and 40 m depth. The half-day

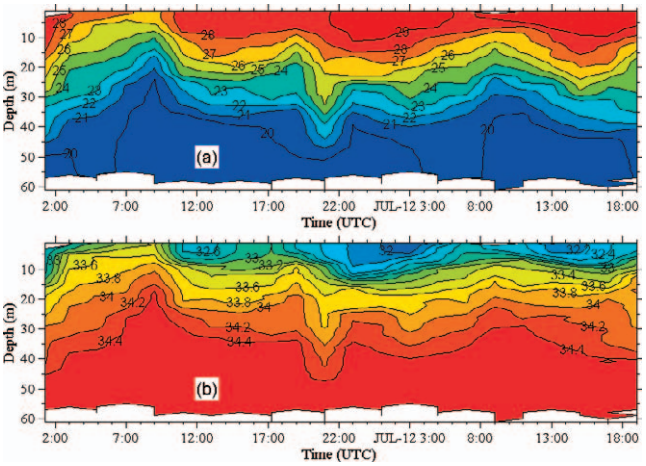

Figure 3. Time-depth variations of temperature (a) and salinity (b) at Sta. A8. The temperature is shown in °C. (Color for this figure is available in the online version of this paper.)

periodic fluctuations of the isotherms presumably due to semidiurnal internal tides are also evident (Hu *et al*., 1999, 2003). Clearly, the variations of the temperature and salinity are highly correlated; increases in temperature corresponded to decreases in salinity, indicating that they were due to the same processes, *i.e*. internal tides. As a result of the strong internal tides, the 21°C isotherm elevates more than 20 m during half of a semidiurnal period (*e.g*. from 0200 to 0900) (Figure 3a), while at the same time, the elevation of the 34.4 isohaline was up to 25 m (Figure 3b). Note that both isothermals and isohalines experienced an abrupt depression during 2000–2200 UTC on 11 July, which is shown in detail later, due to the passage of a packet of HIWs. The sea-surface signature of the waves is shown in Figure 2.

Properties of the HIWs

A high sampling frequency of 8 Hz allows the passage of the HIWs to be captured by the CTD measurements in detail. To visualize local impacts of the internal waves, the time series of temperature and salinity at 33 m depth over the whole observational period are shown in Figure 4. Data from the 22 regular CTD profiling measurements are labeled in circles and connected by a dashed line (Figures 4a and b). The high-frequency variations of temperature and salinity from 2105 to 2209 UTC on 11 July are shown in Figures 4c and d. Clearly, both temperature and salinity had dramatic variations during the 1 hour continuous observational period; the temperature ranged from 27 to 21°C and the salinity ranged from 33.5 to 34.4. Evidently, the variations of temperature and salinity are highly correlated, suggesting that they were both due to the passage of the HIWs. The positive temperature anomaly (Figure 4a) and corresponding negative salinity anomaly (Figure 4b) induced by the waves suggest that the HIWs induced downward displacements of the isothermals and isohalines. This means that the waves were depression internal waves.

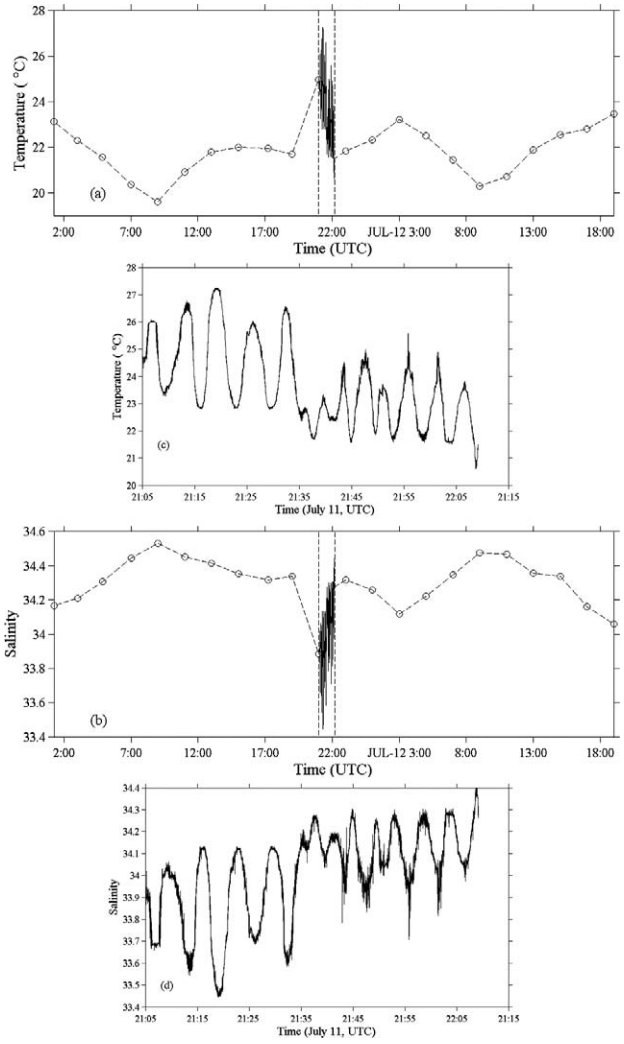

Figure 4. The time series of temperature (a and c) and salinity (b and d) at 33 m depth at Sta. A8.

Note that the decreasing trend of temperature (from 24°C to about 21°C) and increasing trend of salinity (from 34.0 to about 34.4) over the 1 hour period are presumably due to the upward recovery of the isothermals/isohalines after the passage of the trough of the leading big depression wave; the first half of the wave had already passed by the observational site before we started the continuous measurements.

Period of the HIWs

From Figures 4c and d, one can easily identify that there were four crests of the HIWs observed in the first 25 minutes of the 1 hour continuous measurements. Hence, the period of the HIWs is about 6.2 minutes. A more robust estimate from the Fourier-transform–based spectral analysis (Emery and Thomson, 2001) gave a value of 6.4 minutes (385 s) (Figure 5).

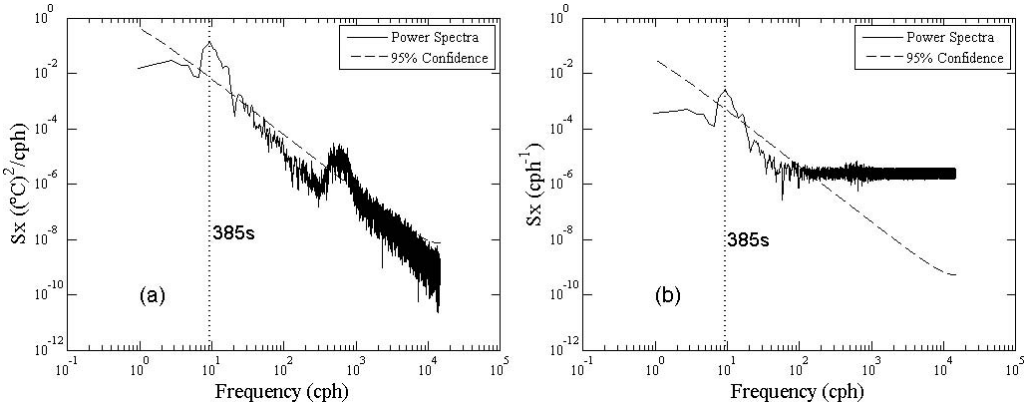

Figure 5. Power spectrum of the temperature (a) and salinity (b) during 2105–2209 UTC on 11 July. The data were collected from the continuous CTD measurements at 33 m depth, with a fast sampling frequency of 8 Hz. The dashed line shows the 95% confidence level.

Amplitude of the HIWs

The perturbations of large-amplitude HIWs can induce large fluctuations of temperature and salinity. Therefore, the amplitude (wave height for harmonic waves, *i.e.* trough to crest distance) of HIWs (ΔZ) can be calculated from CTD measurements at a fixed depth as (Apel *et al.*, 1997)

$$\Delta Z_T = \frac{\Delta T}{R_T}, \tag{1a}$$

$$\Delta Z_S = \frac{\Delta S}{R_S}, \tag{1b}$$

where R_T and R_S are the vertical gradients of temperature (T) and salinity (S) at the measurement depth, *i.e.* $R_T = \partial T/\partial z$ and $R_S = \partial S/\partial z$, and ΔT and ΔS are the amplitudes of temperature and salinity fluctuations, respectively.

To get an accurate estimate of ΔT and ΔS from the continuous CTD measurements by the probe positioned nominally at a fixed depth (about 33 m), we need first to remove the temperature and salinity fluctuations due to depth changes of the probe. As expected, the depth changes were found to be pretty small (about 2 m), and their contributions to the observed temperature and salinity fluctuations were removed by a linear approximation of CTD profiles around the probe's mean depth. In addition, the decreasing trend of temperature and the corresponding increasing trend of salinity presumably due to the recovery process of the passed leading wave also need to be filtered out (Figure 4). The maximum fluctuations ΔT and ΔS were then estimated as 4.5°C and 0.6, respectively. On the other hand, based on the background thermohaline structures shown in Figure 6, the vertical gradients of temperature and salinity R_T and R_S were estimated as 0.2 °C/m and –0.03/m, respectively, with a linear approximation of the CTD profiles. Taken together, the amplitude of the HIWs (ΔZ) was estimated to be about 25 m.

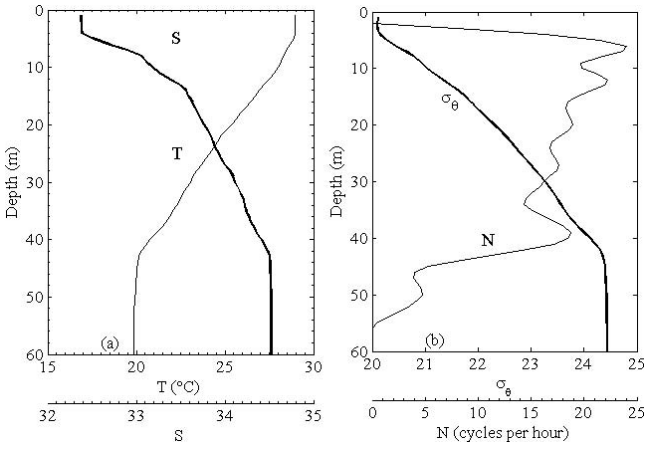

Figure 6. Background thermohaline structures at Sta. A8 before arrival of the HIWs. (a) Temperature (T) and salinity (S), and (b) specific potential density (σ_θ) and buoyancy frequency (N).

Propagation Speed of the HIWs

To estimate the propagation speed of the HIWs, we solved the KdV equation with the observed background stratification. To do this, the realistic density profile was approximated by an equivalent two-layer water-column structure following the methodology of Li *et al.* (2008). Let h_1 and h_2 be the thickness of the upper and lower layers of the water column, respectively, so the quadratic one-dimensional KdV equation has the following form (Jackson, 2009)

$$\eta_t + c_0\eta_x + \alpha\eta\eta_x + \beta\eta_{xx} = 0, \tag{2}$$

where $\eta(x, t)$ is the vertical waveform, c_0 is linear long-wave phase speed, and α and β are the coefficients of nonlinearity and dispersion, respectively. Expresses with the layer thicknesses h_1 and h_2 and the density, these parameters are given by

$$c_0 = \left(g\frac{\Delta\rho}{\rho}\frac{h_1h_2}{h_1+h_2}\right)^{1/2}, \tag{3}$$

$$\alpha = \frac{3}{2}\frac{c_0(h_1-h_2)}{h_1h_2}, \tag{4}$$

$$\beta = \frac{c_0 h_1 h_2}{6}, \tag{5}$$

where g is the acceleration due to gravity, ρ is the averaged density, and $\Delta\rho$ is the density difference between the two layers. The propagation speed of the solitary internal wave is

$$C = c_0 + \frac{\alpha\eta_0}{3}. \tag{6}$$

Here, the CTD data collected half an hour before the arrival of the HIWs were used for the calculation. The background thermohaline structures are shown in Figure 6, based on the upper- and lower-layer thickness of the equivalent two-layer water column, which was estimated to be 10 m and 50 m, respectively. The corresponding densities were 1020.5 kg/m^3 and 1023.0 kg/m^3, respectively. Substituting these values into the above equations, the linear long-wave phase speed was estimated to be 0.45 m/s, and the propagation speed of the HIWs was 0.56 m/s. The eigensolutions of the Strum-Liouville equation (Phillips, 1977), which is valid for weakly nonlinear waves, gave an almost identical value of 0.55 m/s.

DISCUSSION

In the last section, we described the *in situ* observations of internal tides and HIWs at a station at about 60 m depth near the local shelf break in the southern TWS. In particular, the properties of the HIWs were estimated based on the continuous CTD measurements at a fixed point in the pycnocline. The following questions naturally emerge: Where were these waves from? How were they generated? Are they related to the observed internal tides? Here, we try to answer these questions by analyzing a MODIS true color image and conducting a dynamical analysis on the generation mechanism of HIWs based on the perturbed KdV equation (Newell, 1985; Zheng *et al.*, 2007).

Insights from a MODIS True Color Image

As mentioned in the "Observations" section, surface signatures of HIWs in the southern TWS were captured by a MODIS true color image taken at 0515 UTC on 18 July 2010 (Figure 7a). In Figure 7b, the internal wave packets evident in Figure 7a are shown by red lines, which are very close to the observational site A8 represented by a red dot. This coincidence of location means that they should be the same phenomenon at a different time. To have a look at the detailed structure of the internal wave packets in the MODIS image, in Figure 7c we plot the variations of gray scale along the cross-topography red line shown in Figure 7a. It can be seen that the wave packet consists of a leading wave with the largest amplitude followed by trailing waves with decreasing amplitudes. With respect to the *in situ* observations at Sta. A8 (Figures 3 and 4), it is plausible to presume that the observed HIWs are the trailing waves with smaller amplitudes, while the upward movement trend of isothermals and isohalines was due to the passage of the leading wave. It seems from Figure 3 that only the second half (or even less) of the leading wave was captured by the continuous CTD measurements. The upward movement trend of the isothermals and isohalines that is evident in Figure 4 was in fact a result of the recovery process after the passage of the leading wave trough.

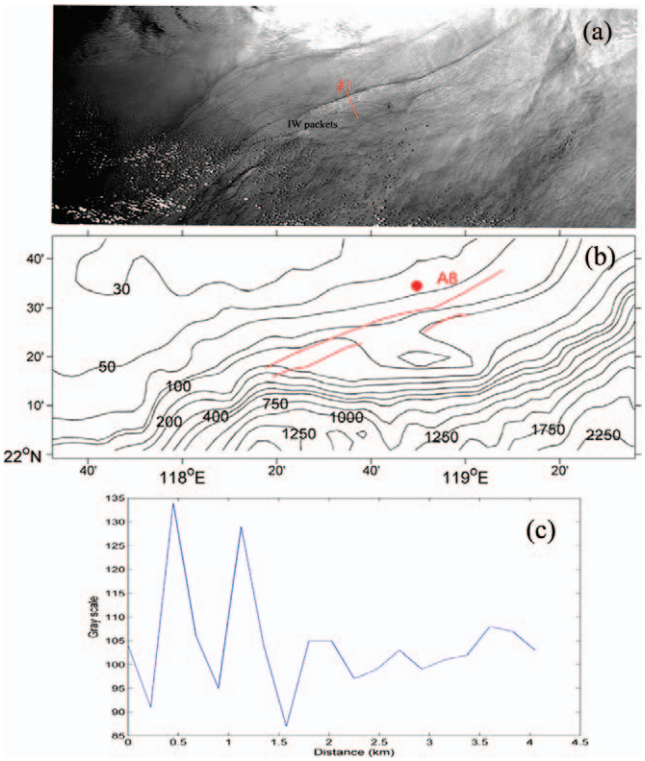

Figure 7. (a) A part of a MODIS true color image in the Taiwan Strait acquired on 18 July 2010 at 0515 UTC (the region is shown with black box in Figure 1). Internal wave packets are visible in the middle of the image. (b) Bathymetry of the image region. The internal wave packets are shown with red lines. (c) The variations of gray scale along the red line shown in (a). (Color for this figure is available in the online version of this paper.)

Dynamical Analysis of the Generation of HIWs

Following the work of Zheng *et al.* (2007), a dynamical analysis on the generation of the HIWs may be conducted based on the perturbed KdV (PKdV) equation,

$$q_\tau + 6qq_\theta + q_{\theta\theta\theta} = -\frac{9}{4}\frac{D_\tau}{D}q, \tag{7}$$

where q is the amplitude of the soliton, τ is a related distance coordinate, and θ is the retarded time. $D\,(=1+H(x)/h_0)$ or $D\,[=1+H(x)/h_0]$ is a nondimensional depth, where h_0 is the maximum water depth, and $-H(x)$ is the height of topography. The subscripts represent partial differentials.

The solutions of Equation (7) can be expressed as

$$q(\theta,\tau) = q^{(0)} + \sigma q^{(1)} + \ldots, \tag{8}$$

which represents a leading soliton, the zero-order solution $q^{(0)}$, with a smaller oscillatory tail, the first-order solution $q^{(1)}$. More details on the equations can be found in Zheng *et al.* (2007).

To study the generation of HIWs due to the shoaling of bottom topography, similar to the case of Zheng *et al.* (2007) for the shoaling of the pycnocline in the open ocean, we have configured a physical model as shown in Figure 8, where the location of Sta. A8 is shown with a black dot. Noticing that the

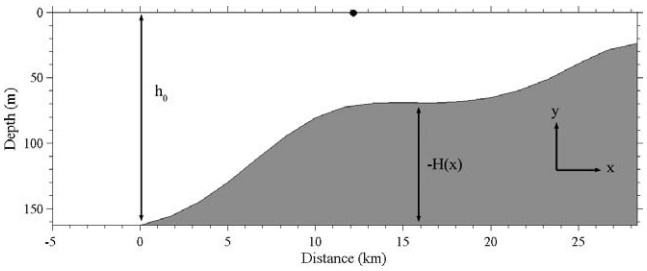

Figure 8. A schematic of the physical model for the generation of HIWs in the continental shelf of the Taiwan Strait. The *y*-axis is upward positive, and the *x*-axis is cross-isobath positive from the deeper region to the shallower region. The location of Sta. A8 is shown with a black dot.

depth of pycnocline is about 40 m, the maximum water depth was chosen as 160 m. The parameters used to determine the solution of the PKdV equation adopted the following values, $\varepsilon = 0.01$, $t = 0$, $\theta = 3$, $\bar{\theta} = 15$, $\sigma = 0.5$, $\eta = 0.4$, and $\Gamma = 0.36$, which were chosen to best represent realistic conditions at Sta. A8 and the adjacent regions.

The solution of the PKdV equation under the above conditions is shown in Figure 9 in the form of spatial wave structure. For comparison, the time series of the isopycnal fluctuations at Sta. A8 were transformed to spatial structures with the propagation speed estimated in the "Properties of the HIWs" section. It can be seen that in general the theoretical model can reproduce the main structure of the observations, suggesting that the observed HIWs may have been generated from the interactions of internal tides and the shoaling bottom topography. However, the validity of this hypothesis needs further observational evidence.

SUMMARY

In this paper, we reported the *in situ* documentation of high-frequency internal wave activities in the southern TWS. The measurements were conducted at a station about 60 m depth near the local shelf break in July 2011. In total, 22 CTD casts separated by 2 hours from each other were taken to obtain the mean and temporal variations of the thermohaline structure due to internal tides, while 1-hour continuous CTD measurements with a probe mounted at a fixed depth in the pycnocline were conducted to study properties of the HIWs. A fast sampling frequency of 8 Hz allowed the structure of the HIWs to be captured in great detail. The waves were found to be depression waves, with a period of about 6.2 min, an amplitude of about 25 m, and a propagation speed of about 0.56 m/s. The HIWs are thought to occur frequently (and maybe in a periodic manner) and presumably are generated by the interactions of the internal tides and the shoaling of bottom topography, based on an analysis of a MODIS true color image and dynamical analysis with the PKdV equation.

ACKNOWLEDGMENTS

This work was jointly supported by the National Basic Research Program of China (2009CB21208) and the National Natural Science Foundation of China (41006017, 40976013, and 41049905). The authors would like to express their appreciation to the crew of R/V *Yanping 2* and all of the cruise participants for help with the fieldwork. We thank three anonymous reviewers for their helpful comments. X. Li was supported by the Shanghai Oriental Scholar Program.

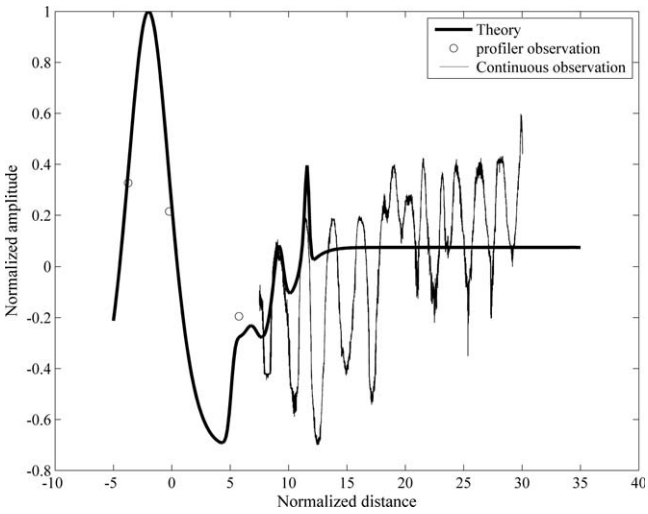

Figure 9. A comparison of the PKdV equation solutions with the *in situ* observations at Sta. A8. The thick line represents theoretical solutions, the thin line is the 1 hour high-frequency continuous measurements, and the black open circles are the CTD profiling data collected about half an hour before arrival of the HIWs.

LITERATURE CITED

Apel, J.R.; Badiey, M.; Chiu, C.S.; Finette, S.; Headrick, R.; Kemp, J.; Lynch, J.F.; Newhall, A.; Orr, M.H.; Pasewark, B.H.; Tielbuerger, D.; Turgut, A.; Heydt, K., and Wolf, S., 1997. An overview of the 1995 SWARM Shallow-Water Internal Wave Acoustic Scattering Experiment. *IEEE Journal of Oceanic Engineering*, 22(3), 465–500.

Cai, S.Q.; Long, X.M.; Dong, D.P., and Wang, S.G., 2008. Background current affects the internal wave structure of the northern South China Sea. *Progress in Natural Science*, 18(5), 585–589.

Cai, S.Q.; Xie, J.S., and He, J.L., 2012. An overview of internal solitary waves in the South China Sea. *Surveys in Geophysics*, 33(5), 927–943.

Colosi, J.A.; Beardsley, R.C.; Lynch, J.F.; Gawarkiewicz, G.; Chiu, C.S., and Scotti, A., 2001. Observations of nonlinear internal waves on the outer New England continental shelf during the summer shelf break primer study. *Journal of Geophysical Research*, 106(C5), 9587–9601.

da Silva, J.C.B.; New, A.L., and Srokosz, M.A., 2002. On the observation of internal tidal waves in remotely-sensed ocean colour data. *Geophysical Research Letters*, 29(12), 1569–1573.

Duda, T.F.; Lynch, J.F.; Irish, J.D.; Beardsley, R.C.; Ramp, S.R.; Chiu, C.S.; Tang, T.Y., and Yang, Y.J., 2004. Internal tide and nonlinear internal wave behavior at the continental slope in the northern South China Sea. *IEEE Journal of Oceanic Engineering*, 29(4), 1105–1130.

Emery, W.J. and Thomson, R.E., 2001. *Data Analysis Methods in Physical Oceanography*. New York: Elsevier, 638p.

Ho, C.R.; Su, F.C., and Zheng, Q.A., 2008. Observations of internal wave in the South China Sea from satellite ocean chlorophyll imagery. *In:* Liu, A. K.; Ho, C.R., and Liu C.T. (eds.), *Satellite Remote Sensing of South China Sea*. Taiwan: Tingmao, pp. 81–94.

Hu, J.Y.; Hong, H.S.; Zhang, X.B.; Chen, Z.Z.; Zhang, C.Y.; Lin, F.Q.; Liang, H.X., and Hong, J.S., 1999. Time series variation of vertical distributions of temperature and salinity in two anchored stations in southern Taiwan Strait in August, 1997. *Journal of Xiamen University (Natural Science)*, 38(5), 732–737 [in Chinese with English abstract].

Hu, J.Y.; Kawamura, H.; Hong, H.S., and Pan, W.R., 2003. A review of research on the upwelling in the Taiwan Strait. *Bulletin of Marine Science*, 73(3), 605–628.

Hu, J.Y.; Kawamura, H.; Li, C.Y.; Hong, H.S., and Jiang, Y.W., 2010. Review on current and seawater volume transport through the Taiwan Strait. *Journal of Oceanography*, 66, 591–610.

Jackson, C.R., 2007. Internal wave detection using the Moderate Resolution Imaging Spectroradiometer (MODIS). *Journal of Geophysical Research*, 112, C11012, doi:10.1029/2007JC004220.

Jackson, C.R., 2009. An empirical model for estimating the geographic location of nonlinear internal solitary waves. *Journal of Atmospheric and Oceanic Technology*, 26(10), 2243–2255.

Lee, C.Y. and Beardsley, R.C., 1974. Generation of long nonlinear internal waves in a weakly stratified shear-flow. *Journal of Geophysical Research*, 79(3), 453–462.

Li, X.F.; Zhao, Z.X.; Han, Z., and Xu, L.X., 2008. Internal solitary waves in the East China Sea. *Acta Oceanologica Sinica*, 27(3), 51–59.

Li, X.F.; Zhao, Z.X., and Pichel, W.G., 2008. Internal solitary waves in the northwestern South China Sea inferred from satellite images. *Geophysical Research Letters*, 35, L13605, doi:10.1029/2008GL034272.

Liu, A.K. and Hsu, M.K., 2004. Internal wave study in the South China Sea using synthetic aperture radar (SAR). *International Journal of Remote Sensing*, 25(7–8), 1261–1264.

Liu, A.K.; Zhao, Y.H., and Hsu, M.K., 2008. Overview of nonlinear internal waves in the South China Sea. *In:* Liu, A. K.; Ho, C.R., and Liu C.T. (eds.), *Satellite Remote Sensing of South China Sea*. Taiwan: Tingmao Publish Company, pp. 1–23.

Newell, A.C., 1985. *Soliton in Mathematics and Physics*. Philadelphia: Society for Industrial and Applied Mathematics, 246p.

Phillips, O.M., 1977. *The Dynamics of the Upper Ocean*. Cambridge: Cambridge University Press, pp. 206–211.

Simmons, H.; Chang, M.H.; Chang, Y.T.; Chao, S.Y.; Fringer, O.; Jackson, C.R., and Ko, D.S., 2011. Modeling and prediction of internal waves in the South China Sea. *Oceanography*, 24(4), 88–99.

Zhao, Z.X.; Klemas, V.; Zheng, Q.A.; Li, X.F., and Yan, X.-H., 2004. Estimating parameters of a two-layer stratified ocean from polarity conversion of internal waves observed in satellite SAR images. *Remote Sensing of Environment*, 92, 276–287.

Zhao, Z.X. and Alford, M.H., 2006. Source and propagation of internal solitary waves in the northeastern South China Sea. *Journal of Geophysical Research*, 111, C11012, doi:10.1029/2006JC003644.

Zheng, Q.A.; Susanto, R.D.; Ho, C.-R.; Song, Y.T., and Xu, Q., 2007. Statistical and dynamical analysis of generation mechanisms of solitary internal waves in the northern South China Sea. *Journal of Geophysical Research*, 112, C03021, doi:10.1029/2006JC003551.

Zheng, Q.A.; Yuan, Y.L.; Klemas, V., and Yan, X.-H., 2001. Theoretical expression for an ocean internal soliton synthetic aperture radar image and determination of the soliton characteristic half width. *Journal of Geophysical Research,* 106(C11), 31415–31423.